

# Phase-Field modeling of brittle fracture of orthotropic materials

Diego Dias Veloso  
Ayrton Ribeiro Ferreira (Prof. Dr.) (Supervisor)

Departamento de Engenharia de Estruturas  
Escola de Engenharia de São Carlos  
Universidade de São Paulo

August 31, 2025

# Topics

## 1 Introduction

- Importance of Fracture Mechanics
- Anisotropic Fracture

## 2 Objectives

## 3 State of the Art

- Griffith Theory
- Phase-Field Method
- Gradient Split

## 4 Computational Implementation

- High-Performance Computing Tools
- Global Minimization
- Linear Momentum Solution
- Damage Solution

## 5 Results

- Single Edge Notch Mode I
- Single Edge Notch Mode II

# Topics (cont.)

- L-Shaped Specimen
- Holed Plate Specimen

6 Partial Conclusions

7 Next Steps

# Introduction

# Importance of Fracture Mechanics

The importance of fracture mechanics can be summarized as follows:

- **Safety:** Predicting failure modes helps prevent catastrophic failures in structures such as bridges, buildings, and aircraft.
- **Material Design:** Insights from fracture mechanics guide the development of new materials with improved toughness and durability.

# Anisotropic Materials

The importance of anisotropic fracture mechanics include:

- **Directional Dependence** : Many engineering materials exhibit anisotropic properties.

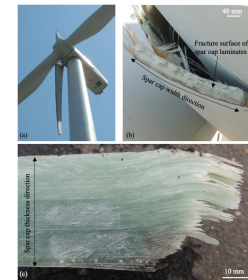
Figure: Examples of anisotropic materials.



(a) Military Aircrafts



(b) Jet Engine Turbo Blade



(c) Wind Turbine

Source: Wikipedia.

# Objectives

# Expected Contributions

The main contributions of this work are:

- **Extend the Ferreira, Marengo e Perego (2024) phase-field model to anisotropic materials.**
- **Implementation of a FEM code on top of HPC techniques.**
- **Validation of the model for orthotropic materials.**
- **Couple the elastic and fracture toughness anisotropies on the fracture process.**

# Schedule

**Table:** Activities to be developed.

No.	Activity description
01	complete the mandatory course credits for the master's program
02	bibliographic review
03	study parallelization libraries: PETSc and ParMETIS
04	implementation of the classical isotropic model of Bourdin, Francfort e Marigo (2000)
05	writing the qualification document
06	qualification exam
07	implementation of the energy decomposition of Ferreira, Marengo e Perego (2024)
08	formulation and implementation of the anisotropic elastic constitutive model
09	formulation and implementation of anisotropic fracture resistance
10	period at the Polytechnic University of Milan, Italy
11	development of numerical examples
12	writing a scientific article for an international journal
13	writing the thesis document
14	defense

Authors.

# Schedule

Table: Activities Timeline.

	2024				2025												2026		
	08	09	10	11	01	02	03	04	05	06	07	08	09	10	11	12	01	02	03
Stage 1																			
Stage 2																			
Stage 3																			
Stage 4																			
Stage 5																			
Stage 6																			
Stage 7																			
Stage 8																			
Stage 9																			
Stage 10																			
Stage 11																			
Stage 12																			
Stage 13																			
Stage 14																			

Authors.

# State of the Art

# Griffith Theory

$$\Pi = U_{elastic} + U_{plastic} + U_{fracture} - W_{ext} \quad , \quad (1)$$

$$\dot{\Pi} = \dot{U}_{elastic} + \dot{U}_{fracture} - \dot{W}_{ext} \quad . \quad (2)$$

For a closed system,  $\dot{\Pi} = 0$ , then the dissipation  $\Phi$  is given by

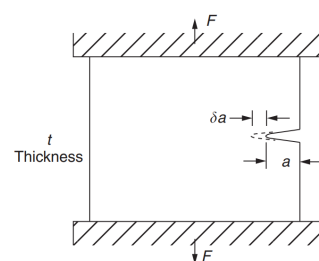
$$\Phi := G\dot{a} = \dot{W}_{ext} - \dot{U}_{elastic} = -\frac{d\Pi}{da}\dot{a} \quad , \quad (3)$$

$$G = -\frac{d\Pi}{da} \quad (4)$$

and Griffith's criterion becomes

$$G \geq G_c \quad , \quad (5)$$

Figure: Body undergoing fracture process.



Source: Jones e Ashby (2019).

# Griffith Theory

and Griffith's criterion becomes

$$G \geq G_c , \quad (6)$$

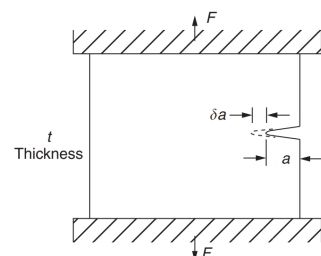
where  $G_c$  is a material Parameter

$$\begin{cases} \dot{a} > 0 \rightarrow G = G_c \\ \dot{a} = 0 \rightarrow G < G_c \end{cases} \quad (7)$$

The critical length of a crack,  $a_c$ , is given by

$$a_c = \frac{2EG_c}{\pi\sigma^2} , \quad (8)$$

Figure: Body undergoing fracture process.



Source: Jones e Ashby (2019).

# Phase-Field Method

The variational recast of the fracture problem leads to

$$\Pi_{int} = \underbrace{\int_{\Omega} \psi(\varepsilon) d\Omega}_{\text{Elastic}} + \underbrace{\int_{\Gamma} G_c dA}_{\text{Dissipation}} . \quad (9)$$

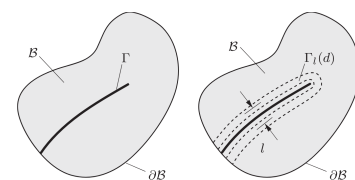
and its regularization by a phase-field  $d$  leads to

$$\Pi_{int} = \int_{\Omega} \psi(\varepsilon, d) d\Omega + \int_{\Omega} \varphi(d, \nabla d) d\Omega . \quad (10)$$

where

$$\begin{cases} \psi(\varepsilon, d) = \omega(d)\psi_0(\varepsilon) \\ \varphi(d, \nabla d) = G_c [w(d) + c_d |\nabla d|^2] \end{cases} \quad (11)$$

**Figure:** (a) Sharp crack surface  $\Gamma$  and (b) the regularized crack region  $\Gamma_l$ .



Miehe, Hofacker e Welschinger  
(2010)

# Phase-Field Method

Strain energy density

$$\psi(\varepsilon, d) = \omega(d)\psi_0(\varepsilon) \quad (12)$$

Quadratic degradation function

$$\omega(d) = (1 - d)^2 \quad (13)$$

Dissipation density

$$\varphi(d, \nabla d) = G_c \left[ w(d) + c_d |\nabla d|^2 \right] \quad (14)$$

where

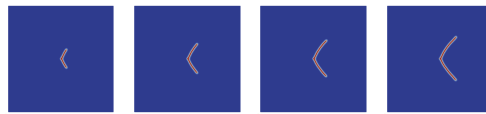
$$w(d) = \begin{cases} \frac{3}{8l_0}d & \text{AT1} \\ \frac{1}{2l_0}d^2 & \text{AT2} \end{cases} \quad (15)$$

$$c_d = \begin{cases} \frac{3}{8}l_0 & \text{AT1} \\ \frac{1}{2}l_0 & \text{AT2} \end{cases} . \quad (16)$$

# Assymmetric Elastic Strain Energy Degradation

Symmetric degradation of the strain energy density

**Figure:** SEN Mode II - Specimen with interpenetration due to symmetric elastic strain energy degradation.



**Source:** Authors.

Assymmetric degradation of the strain energy density  $\rightarrow \psi(\varepsilon, d) = \omega(d)\psi_0^+(\varepsilon) + \psi_0^-(\varepsilon)$

**Volumetric-Deviatoric Split**

$$\psi_0^\pm(\varepsilon) = H^\pm(\text{Tr}(\varepsilon)) \frac{\kappa}{2} (\text{Tr}(\varepsilon))^2 + \mu \varepsilon_D : \varepsilon_D \quad (17)$$

# Gradient Energy Split

$$\psi(\boldsymbol{\varepsilon}, d) = \int_{\Omega} [\omega(d) + [1 - \omega(d)] H^-(\sigma_{0n})] \psi_0(\boldsymbol{\varepsilon}) d\Omega , \quad (18)$$

where

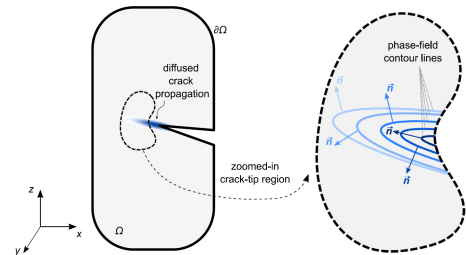
$$\sigma_{0n} = \boldsymbol{\sigma} : \mathbf{n} \otimes \mathbf{n} . \quad (19)$$

and the projection direction is given by

$$\mathbf{n} := \begin{cases} -\frac{\nabla d}{\|\nabla d\|} & \text{if } \nabla d \neq 0 \\ 0 & \text{if } \nabla d = 0 \end{cases} \quad (20)$$

$$\sigma_{0n} := \begin{cases} \boldsymbol{\sigma} : \mathbf{n} \otimes \mathbf{n} & \text{if } \nabla d \neq 0 \\ \text{Tr}(\boldsymbol{\sigma}) & \text{if } \nabla d = 0 \end{cases} \quad (21)$$

**Figure:** Normal to crack direction.



# Computational Implementation

# High-Performance Computing Tools

The following high-performance computing tools are utilized in the implementation:

- **PETSc**: A suite of data structures and routines for the scalable (parallel) solution of scientific applications modeled by partial differential equations.
- **METIS**: A software package for partitioning unstructured graphs and computing fill-reducing orderings of sparse matrices.
- **GMSH**: A 3D finite element mesh generator with built-in pre- and post-processing facilities.
- **Python**: A programming language used for scripting and automation of the workflow.
- **Paraview**: An open-source, multi-platform data analysis and visualization application.

# PETSc



PETSc (Portable, Extensible Toolkit for Scientific Computation) is designed for the **scalable** solution of scientific applications modeled by partial differential equations (**PDEs**). It is a powerful and convenient interface for:

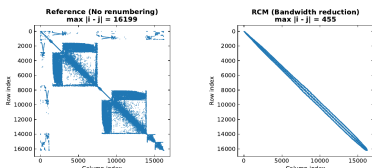
- Management of **parallelism and communication**.
- **Algebraic operations** on distributed vectors (Vec) and matrices(Mat).
- Linear (KSP) and nonlinear (SNES) **solvers** (algorithms (NR, LS, TR, etc) based on KSP objects).

# METIS

METIS is a library for partitioning and producing fill reducing orderings for finite element meshes.

- **Fill-reducing:** METIS\_NodeND.
- **Mesh Partitioning:** METIS\_PartMeshDual.

Figure: Sparse matrix representation.



Authors.

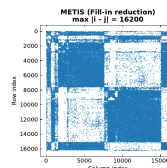
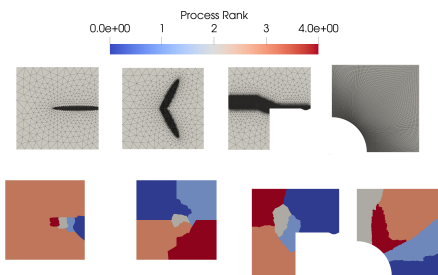


Figure: Mesh partitioning.



Authors.

# GMSH,HDF5, Python, Paraview

- **GMSH:** A 3D finite element mesh generator with built-in pre- and post-processing facilities.
- **HDF5:** Built for fast I/O processing and storage.
- **Python:** A programming language used for scripting and automation of the workflow.
- **Paraview:** Open-source multiple-platform application for interactive, scientific visualization.

[Figure:](#) Mesh partitioning.



Authors.

# Solution of the coupled problem

- **Monolithic approach** (BHARALI et al., 2022)

$$\begin{bmatrix} \mathbf{K}^{uu} & \mathbf{K}^{ud} \\ \mathbf{K}^{du} & \mathbf{K}^{dd} \end{bmatrix} \begin{bmatrix} \Delta \mathbf{u} \\ \Delta d \end{bmatrix} = \begin{bmatrix} \mathbf{r}^u \\ \mathbf{r}^d \end{bmatrix} \quad (22)$$

- **Staggered approach**

$$\begin{bmatrix} \mathbf{K}^{uu} & 0 \\ 0 & \mathbf{K}^{dd} \end{bmatrix} \begin{bmatrix} \Delta \mathbf{u} \\ \Delta d \end{bmatrix} = \begin{bmatrix} \mathbf{r}^u \\ \mathbf{r}^d \end{bmatrix} \quad (23)$$

or, in more detail,

$$\begin{cases} \partial_u \Pi_{n+1}(\mathbf{u}_{n+1}^{i+1}, d_{n+1}^i) = 0 \\ \partial_d \Pi_{n+1}(\mathbf{u}_{n+1}^{i+1}, d_{n+1}^{i+1}) [\Delta d_{n+1}^{i+1}] = 0, \quad \partial_d \Pi_{n+1}(\mathbf{u}_{n+1}^{i+1}, d_{n+1}^{i+1}) \geq 0, \quad \Delta d_{n+1}^{i+1} \geq 0 \end{cases} \quad . \quad (24)$$

# Staggered approach

**Require:** Load solution  $(\mathbf{u}_n, d_n)$  from step  $n$  and boundary conditions  $g_{n+1}, t_n$  at current step  $n$

- 1: initialize  $i \leftarrow 0$
- 2: set  $(\mathbf{u}^0, d^0) \leftarrow (\mathbf{u}_n, d_n)$
- 3: **while**  $Re_{\text{stag}} \geq TOL_{\text{stag}}$  **do**
- 4:      $i \leftarrow i + 1$
- 5:     given  $d^{i-1} = d_n + \Delta d^{i-1}$ , find  $\mathbf{u}^i$  solving  $\partial_{\mathbf{u}} \Pi_{n+1}(\mathbf{u}^i, d^{i-1}) = 0$
- 6:     given  $\mathbf{u}^i$ , find  $\Delta d^i$  solving  $\partial_d \Pi_{n+1}(u^i, d_n)[\Delta d^i] = 0$  with  $\partial_d \Pi_{n+1}(\mathbf{u}^i, d_n) \geq 0$ ,  $\Delta d^i \geq 0$
- 7:     compute  $|Re_{\text{stag}} = \partial_{\mathbf{u}} \Pi_{n+1}(\mathbf{u}^i, d^i)[\Delta \mathbf{u}^i]|$
- 8: **end while**
- 9:  $(\mathbf{u}_{n+1}, d_{n+1}) \leftarrow (\mathbf{u}^i, d^i)$

# Linear Momentum Solution

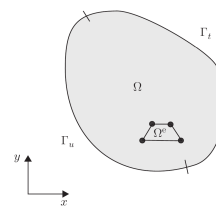
From Principle of Virtual Work, the weak form is given as:

$$\int_{\Omega} [\nabla^s \mathbf{w} : \mathbb{D} \nabla^s \mathbf{u}] dV = \int_{\Gamma_t} \mathbf{t} \cdot \mathbf{w} dS + \int_{\mathcal{B}} \mathbf{b} \cdot \mathbf{w} dV \quad \forall \mathbf{w} = 0 \text{ on } \Gamma_u \quad (25)$$

$$\begin{cases} \mathbf{u}(x, y) = \mathbf{N}^e(x, y) \mathbf{u}^e \\ \mathbf{w}(x, y) = \mathbf{N}^e(x, y) \mathbf{w}^e \end{cases} \quad \forall (x, y) \in \Omega_e \quad (26)$$

$$\boldsymbol{\varepsilon} = \nabla^s \mathbf{u} = \mathbf{B}^e \mathbf{u}^e \quad (27)$$

Figure: Discrete domain.



and the system of equations can be written as

$$\mathbf{K} \mathbf{u} = \mathbf{F} \quad (28)$$

where

$$\mathbf{K} = \sum_{e=1}^n \left[ \int_{\Omega_e} \mathbf{B}_e^T \mathbb{C} \mathbf{B}_e d\Omega \right] \mathbf{u}^e \quad \text{and} \quad \mathbf{F} = \sum_{e=1}^n \int_{\Gamma_e} \mathbf{N}_e^T \mathbf{t} d\Gamma + \sum_{e=1}^n \int_{\Omega_e} \mathbf{N}_e^T \mathbf{b} d\Omega \quad (29)$$

Anand e Govindjee (2020).

# Newton Raphson

Taylor expansion gives

$$\mathbf{R}(\mathbf{u}^{k+1}) = \mathbf{R}(\mathbf{u}^k) + \left[ \frac{\partial \mathbf{R}}{\partial \mathbf{u}} \right]_{\mathbf{u}^k} (\mathbf{u}^{k+1} - \mathbf{u}^k) + \mathcal{O} \left( (\mathbf{u}^{k+1} - \mathbf{u}^k)^2 \right) \quad (30)$$

that, after linearization and assuming that  $\mathbf{R}(\mathbf{u}^{k+1}) = 0$

$$\mathbf{R}(\mathbf{u}^k) + \left[ \frac{\partial \mathbf{R}}{\partial \mathbf{u}} \right]_{\mathbf{u}^k} (\mathbf{u}^{k+1} - \mathbf{u}^k) = 0 \quad , \quad (31)$$

Rearranging the equation, we can write

$$\left[ \frac{\partial^2 \Pi}{\partial \mathbf{u}^2} \right]_{\mathbf{u}^k} \Delta \mathbf{u}^{k+1} = -\mathbf{R}(\mathbf{u}^k) \quad \Rightarrow \quad \mathbf{K}(\mathbf{u}^k) \Delta \mathbf{u}^{k+1} = -\mathbf{R}(\mathbf{u}^k) \quad (32)$$

PCFactorSetReuseOrdering(PETSC\_TRUE) and KSPSetReusePreconditioner(PETSC\_FALSE)

# Line Search

Optimal step size

$$\mathbf{u}_n^{k+1} = \mathbf{u}^k + \eta_n \Delta \mathbf{u}^{k+1} \quad . \quad (33)$$

assuming that  $\mathbf{R}(\eta_n) \perp \Delta \mathbf{u}$

$$\mathbf{R}(\eta_n) = \mathbf{R}(\eta_n) \cdot \Delta \mathbf{u} = \mathbf{R}(\mathbf{u}^k + \eta_n \Delta \mathbf{u}) \cdot \Delta \mathbf{u} \quad (34)$$

that, after some algebra, leads to the following iterative formula for  $\eta$ :

$$\eta_{n+1} = \begin{cases} \frac{\alpha_n}{2} + \sqrt{\left(\frac{\alpha_n}{2}\right)^2 - \alpha_n} & \text{if } \alpha_n < 0 \\ \frac{\alpha_n}{2} & \text{if } \alpha_n > 0 \end{cases} \rightarrow \text{where } \alpha_n = \frac{\mathbf{R}(\mathbf{u}^k)}{\mathbf{R}(\eta_n)} = \frac{R_0}{R(\eta_n)} \quad (35)$$

with a stopping criterion defined by Bonet, Gil e Wood (2016) as

$$|R(\eta_n)| < \rho |R(0)| \quad , \quad \text{which } \rho = 0.5 \quad (36)$$

**Ensure:** Newton-raphson solution  $\Delta\mathbf{u}^{k+1}$

```
1: Compute  $R_0 = \mathbf{R}(\mathbf{u}^k) \cdot \Delta\mathbf{u}^{k+1}$ 
2:  $\eta_0 \leftarrow 1$ ,  $\rho \leftarrow 0.5$ 
3: for  $n = 0$  to  $N_{\max}^{LS}$  do
4:    $\mathbf{u}_n \leftarrow \mathbf{u}^k + \eta_n \Delta\mathbf{u}^{k+1}$ 
5:   Assemble residual  $\mathbf{R}(\eta_n) = \mathbf{F}(\eta_n)_{int} - \mathbf{F}_{ext}$ 
6:   Compute  $R(\eta_n) = \mathbf{R}(\eta_n) \cdot \Delta\mathbf{u}^{k+1}$ 
7:   if  $|R(\eta_n)| \leq \rho |R_0|$  then
8:     break
9:   else
10:     $\alpha \leftarrow R_0 / R(\eta_n)$ 
11:    if  $\alpha < 0$  then
12:       $\eta_n \leftarrow \alpha/2 + \sqrt{(\alpha/2)^2 - \alpha}$ 
13:    else
14:       $\eta_n \leftarrow \alpha/2$ 
15:    end if
16:   end if
17:    $n \leftarrow n + 1$ 
18: end for
19:  $\mathbf{u}^{k+1} \leftarrow \mathbf{u}^k + \eta_n \Delta\mathbf{u}^{k+1}$ 
```

# Symmetric Linear Complementarity Problem (SLCP)

Taylor expansion around  $\hat{\mathbf{d}}_n$

$$\Pi_{n+1}(\hat{\mathbf{u}}^i, \hat{\mathbf{d}}) = \frac{1}{2} \Delta \hat{\mathbf{d}}^\top Q^i \Delta \hat{\mathbf{d}} + \Delta \hat{\mathbf{d}}^\top q^i + \Pi_{n+1}(\hat{\mathbf{u}}^i, \hat{\mathbf{d}}_n), \quad (37)$$

where

$$\Delta \hat{\mathbf{d}} = \hat{\mathbf{d}} - \hat{\mathbf{d}}_n, \quad Q^i = \nabla_{\hat{\mathbf{d}} \hat{\mathbf{d}}}^2 \Pi_{n+1}(\hat{\mathbf{u}}^i, \hat{\mathbf{d}}_n), \quad q^i = \nabla_{\hat{\mathbf{d}}} \Pi_{n+1}(\hat{\mathbf{u}}^i, \hat{\mathbf{d}}_n). \quad (38)$$

and finally, the Jacobian (Hessian)  $Q^i$  and Gradient(Residue)  $q^i$  are given by

$$Q^i := \Psi_e(\hat{\mathbf{u}}^i) + G_c \Phi_e, \quad q^i := Q^i \hat{\mathbf{d}}_n - \psi_e(\hat{\mathbf{u}}^i). \quad (39)$$

# Symmetric Linear Complementarity Problem (SLCP)

the constant element dissipation matrix  $\Phi_e$  is given by

$$\Phi_e := \begin{cases} \int_{\Omega_e} \left( \frac{3l_0}{8} B_{d,e}^T B_{d,e} \right) d\Omega_e & \text{if AT1} \\ \int_{\Omega_e} \left( l_0^{-1} N_{d,e}^T N_{d,e} + l_0 B_{d,e}^T B_{d,e} \right) d\Omega_e & \text{if AT2} \end{cases} \quad (40)$$

and the element free energy matrix  $\Psi_e$  and vector  $\psi_e$  are given by

$$\Psi_e(\hat{\mathbf{u}}_e^i) := \int_{\Omega_e} 2 \psi_0^+(\hat{\mathbf{u}}_e^i) N_{d,e}^T N_{d,e} d\Omega_e \quad (41)$$

$$\psi_e(\hat{\mathbf{u}}_e^i) := \begin{cases} \int_{\Omega_e} \left[ 2 \psi_0^+(\hat{\mathbf{u}}_e^i) - \frac{3l_0}{8} \right] N_{d,e}^T d\Omega_e. & \text{if AT1} \\ \int_{\Omega_e} 2 \psi_0^+(\hat{\mathbf{u}}_e^i) N_{d,e}^T d\Omega_e. & \text{if AT2} \end{cases} \quad (42)$$

# Projected Successive Over-Relaxation (PSOR)

The SLCP is gives rise to the following conditions:

$$\partial_d \Pi_{n+1}(\mathbf{u}_{n+1}, d_{n+1}) [\Delta d_{n+1}], \quad \partial_d \Pi_{n+1}(\mathbf{u}_{n+1}, d_{n+1}) \geq 0, \quad \Delta d_{n+1} \geq 0 \quad (43)$$

$$x^{k+1} = (\mathbf{L} + \mathbf{D})^{-1} (b - \mathbf{U}x^k) \quad (44)$$

which, after some algebra, Marengo et al. (2021) shows that can be written as

$$\Delta d_r^k = \left\langle \Delta d_r^{k-1} - D_{rr}^{-1} \left[ Q_{rc} \Delta d_c^{k-1} + L_{rc} (\Delta d_c^k - \Delta d_c^{k-1}) \right] \right\rangle_+ \quad (45)$$

where

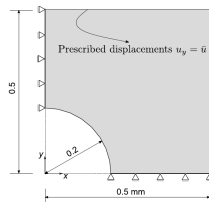
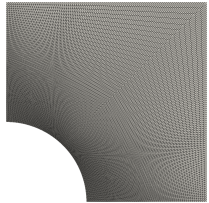
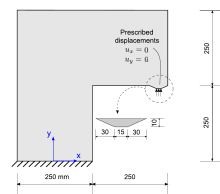
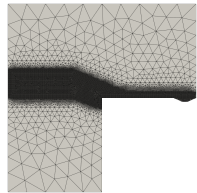
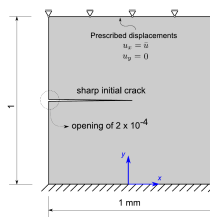
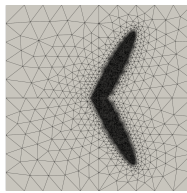
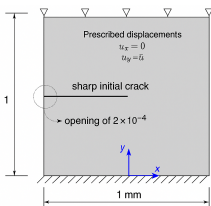
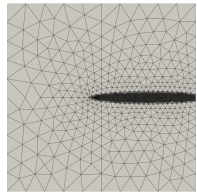
$$\begin{cases} L_{rc} := Q_{r>c} \\ D_{rr} := Q_{r=r} \end{cases} \quad (46)$$

$$\langle x \rangle_+ := \begin{cases} x & \text{if } x \geq 0 \\ 0 & \text{if } x < 0 \end{cases} \quad (47)$$

# Results

# Physical Properties for Benchmark Examples

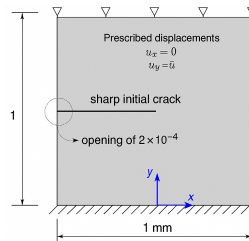
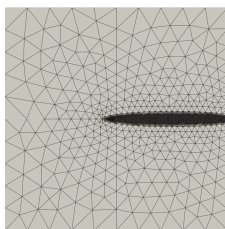
Figure: Benchmarks.



Authors.

# Single Edge Notch Mode I

Figure: Geometry and boundary conditions.



Imposed cyclic displacement

$$\Delta \bar{u}_n = \begin{cases} 4 \times 10^{-3} \text{ mm} & \text{if } 1 \leq n \leq 20 \\ -4 \times 10^{-4} \text{ mm} & \text{if } 21 \leq n \leq 60 \\ 4 \times 10^{-4} \text{ mm} & \text{if } 61 \leq n \leq 80 \end{cases}$$

Source: Ferreira, Marengo e Perego (2024).

Table: Physical properties for benchmark examples.

Example	$E$ GPa	$\nu$	$G_c$ N/mm	$\ell_0$ mm
SEN Mode I	210	0.3	2.7	0.01

Source: Authors.

Figure: Specimen with load reversal.



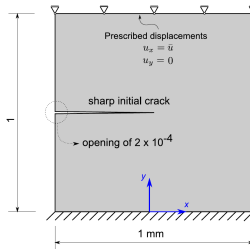
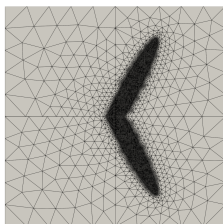
Figure: Reaction forces.

Source: Authors.

Source: Authors.

# Single Edge Notch Mode II

Figure: Geometry and boundary conditions.



The imposed cyclic loading for this case is:

$$\Delta \bar{u}_n = \begin{cases} 1 \times 10^{-3} \text{ mm} & \text{if } 1 \leq n \leq 6 \\ 3 \times 10^{-4} \text{ mm} & \text{if } 7 \leq n \leq 26 \\ -3 \times 10^{-4} \text{ mm} & \text{if } 27 \leq n \leq 106 \\ 3 \times 10^{-4} \text{ mm} & \text{if } 107 \leq n \leq 146 \end{cases}$$

Source: Ferreira, Marengo e Perego (2024).

Table: Physical properties for benchmark examples.

Example	$E$ GPa	$\nu$	$G_c$ N/mm	$\ell_0$ mm
SEN Mode II	210	0.3	2.7	0.01

Source: Authors.

**Figure:** Specimen with load reversal.



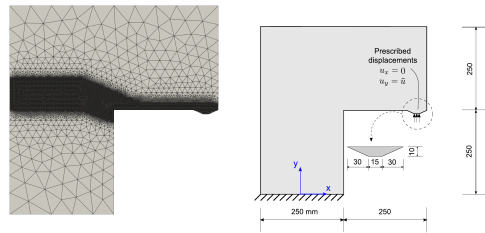
**Figure:** Reaction forces.

**Source:** Authors.

**Source:** Authors.

# L-Shaped Specimen

Figure: Geometry and boundary conditions.



Subjected to the following displacement history:

$$\Delta \bar{u}_n = \begin{cases} 1 \times 10^{-2} \text{ mm} & \text{if } 1 \leq n \leq 36 \\ -3 \times 10^{-2} \text{ mm} & \text{if } 37 \leq n \leq 48 \\ -1 \times 10^{-2} \text{ mm} & \text{if } 49 \leq n \leq 84 \\ 3 \times 10^{-2} \text{ mm} & \text{if } 85 \leq n \leq 96 \end{cases}$$

Figure: Ferreira, Marengo e Perego (2024).

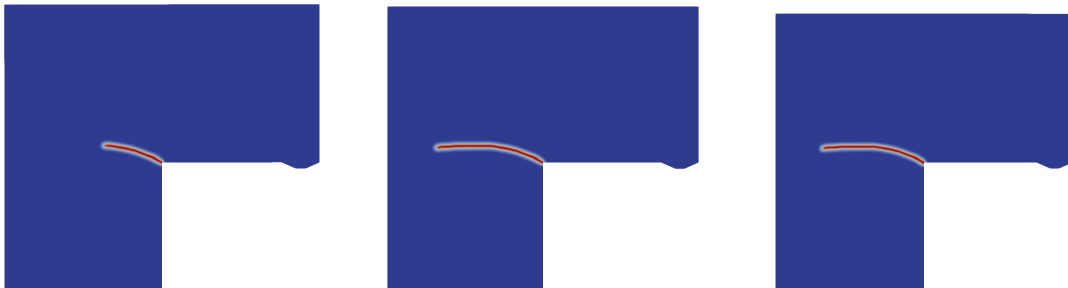
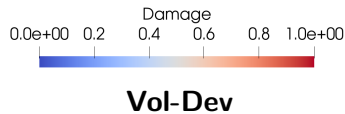
Table: Physical properties for benchmark examples.

Example	$E$ GPa	$\nu$	$G_c$ N/mm	$\ell_0$ mm
L-Shaped	25.85	0.18	0.095	5.0

Source: Authors.

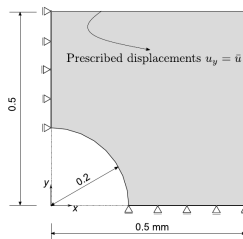
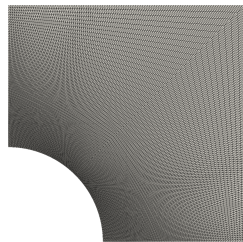
# L-Shaped Specimen

**Figure:** L-Shaped - Specimen with load reversal. AT1 phase-field contours at three different time steps (or last converged step for the Vol–Dev split).



# Holed Plate Specimen

Figure: Geometry and boundary conditions.



The imposed cyclic loading is specified as:

$$\Delta\bar{u}_n = \begin{cases} 1 \times 10^{-2} \text{ mm} & \text{if } 1 \leq n \leq 301 \\ 3 \times 10^{-2} \text{ mm} & \text{if } 302 \leq n \leq 903 \end{cases}$$

Figure: Ferreira, Marengo e Perego (2024).

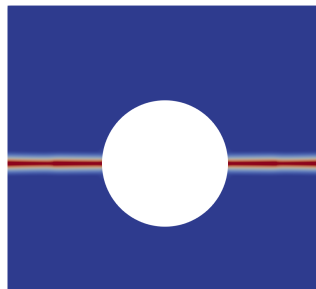
Table: Physical properties for benchmark examples.

Example	$E$ GPa	$\nu$	$G_c$ N/mm	$\ell_0$ mm
Holed Plate	210	0.3	2.7	0.02

Source: Authors.

# Holed Plate Specimen

**Figure:** Holed Plate - Specimen with load reversal. AT1 phase-field contours at different time steps (or last converged step for the Vol–Dev split).



# Partial Conclusions

# Results

The main contributions of this thesis are:

- Anisotropic phase-field damage formulation for elastic and fracture **anisotropy**.
- A parallel FEM code using **HPC** techniques and tools.
- Identification of model-implementation **limitations** and proposals for **extensions** (e.g., Drucker-Prager criteria and alternative energy splits).

The following key observations were made:

- The model closely **approximated the crack path and peak load** within the Vol-Dev model reference.
- The model **captured the load reversal** behavior accurately.
- The model is directly **extensible to anisotropic materials**.

# Results

Despite the successful implementation and validation, some limitations remain:

- **Fixing  $H^-$  during staggered iterations.** In the current staggered solution strategy the negative Heaviside field  $H^-$  is held fixed until the minimum residual is reached, unlike the volumetric–deviatoric (Vol–Dev) split where  $H^-$  is allowed to evolve.
- **Energy split formulation and compressive fracture.** The present energy split does not represent fracture initiation under primarily compressive stress states. A possible remedy is to incorporate a Drucker–Prager type criterion.
- **Solver and scalability improvements.** While MPI provides good scalability, introducing better preconditioners and iterative solvers could further improve performance.

# Next Steps

# Next Steps

The next steps to be taken are:

- Validate the implementation of the transversely isotropic and orthotropic anisotropies of the constitutive tensor;
- Develop validation tests for transversely isotropic and orthotropic materials symmetries;
- Validate the implementation of the weak anisotropy model;
- Write an international paper for a high impact journal;
- Implement an efficient solver for the implemented strong anisotropy model;
- If possible: Development of at least one 3D example with trigonal symmetry.

# References

ANAND, L.; GOVINDJEE, S. **Continuum Mechanics of Solids**. 1. ed. Oxford University PressOxford, 2020. ISBN 978-0-19-886472-1 978-0-19-189676-7. Disponível em: <<https://academic.oup.com/book/43650>>.

BHARALI, R. et al. A robust monolithic solver for phase-field fracture integrated with fracture energy based arc-length method and under-relaxation. **Computer Methods in Applied Mechanics and Engineering**, v. 394, p. 114927, maio 2022. ISSN 00457825. Disponível em: <<https://linkinghub.elsevier.com/retrieve/pii/S0045782522001992>>.

BONET, J.; GIL, A. J.; WOOD, R. D. **Nonlinear Solid Mechanics for Finite Element Analysis: Statics**. 1. ed. Cambridge University Press, 2016. ISBN 978-1-107-11579-8 978-1-316-33614-4. Disponível em: <<https://www.cambridge.org/core/product/identifier/9781316336144/type/book>>.

## References (cont.)

- BOURDIN, B.; FRANCFORTE, G.; MARIGO, J.-J. Numerical experiments in revisited brittle fracture. **Journal of the Mechanics and Physics of Solids**, v. 48, n. 4, p. 797–826, abr. 2000. ISSN 00225096. Disponível em: <doi:10.1016/S0022-5096(99)00028-9>.
- FERREIRA, A. R.; MARENKO, A.; PEREGO, U. A phase-field gradient-based energy split for modeling of brittle fracture under cyclic loading. **(under revision)**, 2024.
- JONES, D. R. H.; ASHBY, M. F. **Engineering materials 1: an introduction to properties, applications and design**. Fifth edition. Oxford, United Kingdom: Butterworth-Heinemann, 2019. ISBN 978-0-08-102051-7.
- MARENKO, A. et al. A rigorous and efficient explicit algorithm for irreversibility enforcement in phase-field finite element modeling of brittle crack propagation. **Computer Methods in Applied Mechanics and Engineering**, p. 114137, dez. 2021. ISSN 00457825. Disponível em: <<https://linkinghub.elsevier.com/retrieve/pii/S0045782521004680>>.

## References (cont.)

MIEHE, C.; HOFACKER, M.; WELSCHINGER, F. A phase field model for rate-independent crack propagation: Robust algorithmic implementation based on operator splits. **Computer Methods in Applied Mechanics and Engineering**, v. 199, n. 45-48, p. 2765–2778, nov. 2010. ISSN 00457825. Disponível em: <doi:10.1016/j.cma.2010.04.011>.